ELECTRON CYCLOTRON RESONANCE HEATING ON TEXTOR

E. WESTERHOF,*† J. A. HOEKZEMA,‡ G. M. D. HOGEWEIJ,† R. J. E. JASPERS,† F. C. SCHÜLLER,† C. J. BARTH,† H. BINDSLEV,†§ W. A. BONGERS,† A. J. H. DONNÉ,† P. DUMORTIER,‖ A. F. VAN DER GRIFT,† D. KALUPIN,‖ H. R. KOSLOWSKI,‡ A. KRÄMER-FLECKEN,‡ O. G. KRUIJT,† N. J. LOPES CARDOZO,† H. J. VAN DER MEIDEN,† A. MERKULOV,† A. MESSIAEN,‖ J. W. OOSTERBEEK,‡ P. R. PRINS,† J. SCHOLTEN,† V. S. UDINTSEV,† B. UNTERBERG,‡ M. VERVIER,‖ and G. VAN WASSENHOVE‖

†*FOM-Institute for Plasma Physics Rijnhuizen, Association EURATOM-FOM, Trilateral Euregio Cluster P.O. Box 1207, 3430 BE Nieuwegein, The Netherlands (⟨www.rijnh.nl⟩)*

‡*Institut für Plasmaphysik, Forschungszentrum Jülich GmbH, EURATOM Association, Trilateral Euregio Cluster D-52425 Jülich, Germany*

§*Optics and Fluid Dynamics Department, Ass. Euratom-National Laboratory Risø, DK-4000 Roskilde, Denmark*

‖*Laboratory for Plasma Physics, Ecole Royale Militaire-Koninklijke Militaire School Association EURATOM-Belgian State, Trilateral Euregio Cluster, B-1000 Brussels, Belgium*

Received April 29, 2004
Accepted for Publication July 26, 2004

TEXTOR is equipped with two gyrotrons at 110 and 140 GHz, respectively. Both share a single power supply and a confocal quasi-optical transmission line. They cannot be operated simultaneously. The 110-GHz gyrotron with limited power and pulse length (300 kW; 200 ms) has been used in a first series of experiments on electron cyclotron resonance heating (ECRH) and electron cyclotron current drive (ECCD) and for collective Thomson scattering (CTS) diagnostics of energetic ions. In the future the 110-GHz gyrotron will be operated exclusively for CTS diagnostics, while for ECRH and ECCD, the newly installed 140-GHz, high-power (800-kW), long-pulse (>3-s) gyrotron is now available. The highlights of first ECRH experiments with the 110-GHz gyrotron are reported. These include observations of internal transport barriers with ECRH on various target plasmas: in the current plateau phase of both ohmic and radiation improved mode (RI-mode) discharges. In addition, sawtooth control by localized ECRH is demonstrated. First results on CTS include the observation of the slowing down of energetic ions and of the redistribution of energetic ions in sawtooth crashes.

KEYWORDS: *electron cyclotron resonance heating, electron cyclotron current drive, collective Thomson scattering*

I. INTRODUCTION

Electron cyclotron resonance heating (ECRH) and electron cyclotron current drive (ECCD) use the resonance between an electromagnetic wave and the gyration of the electrons around the magnetic field to transfer energy from the waves to the electrons. Because of the high frequency (of the order of 100 GHz) and, consequently, small wavelength of the waves, the waves can be injected in relatively narrow and well-focused beams. The combination of these narrow beams with the well-localized resonant wave particle interaction results in a very small volume of power deposition. For example, in TEXTOR (major radius $R_0 = 1.75$ m; minor radius $a = 0.46$ m) with a beam radius in the center of the plasma of $\sim$1 cm and an absorption length of 1 to 2 cm, a power of up to 800 kW is deposited in a volume of only 10 cm^3. Even in terms of flux surfaces, all power is deposited within a width of $\Delta\rho \approx 0.05$, where ρ is the normalized minor radius. This unique property makes ECRH and ECCD ideally suited for studies or control of local transport and the control of plasma profiles and instabilities.

*E-mail: e.westerhof@rijnh.nl

Reviews of ECRH and ECCD have been published in (Refs. 1, 2, and 3).

First activities in the field of ECRH and ECCD at the FOM-Institute for Plasma Physics Rijnhuizen (FOM-Rijnhuizen) started in the early 1980s, when a small group of physicists and technicians joined the Princeton Divertor Experiment[4] (PDX). The experience gained on PDX was then applied to a major ECRH experiment on the Tokamak a Fontenay aux Roses (TFR) near Paris, which at that time was a medium-sized machine. In 1983, three 60-GHz, 200-kW, 100-ms Varian gyrotrons were installed on TFR. This made it one of the most powerful ECRH systems of that time. Many of the ECRH and ECCD physics applications addressed at TFR (Ref. 5) are still at the heart of ECRH programs worldwide. These include good central confinement with ECRH, measurement of electron energy transport through modulated ECRH, the control of sawteeth and tearing modes, etc.[2,3] The ECRH program on TFR ended with the closure of the tokamak in 1987.

At the same time, it was decided to concentrate all FOM-Rijnhuizen fusion research on a single in-house experiment: the Rijnhuizen Tokamak Project (RTP). It was natural that ECRH would provide its additional heating. Two of the three 60-GHz gyrotrons from TFR were installed at RTP and later were replaced by a single 110-GHz, 500-kW, 200-ms Gycom gyrotron. Thanks to the combination of highly localized, high-power electron heating and high-resolution electron diagnostics, RTP was able to make some remarkable contributions to tokamak physics. These include among others the observation of transport barriers associated with surfaces with rational safety factors as the ECRH power deposition is scanned through the plasma,[6] the stabilization by ECRH of tearing modes that otherwise would have resulted in disruptive termination of the discharge,[7] and the demonstration through modulated ECRH of a possible inward heat pinch associated with the transport barrier at the $q = 1$ surface.[8]

In 1997, FOM-Rijnhuizen joined forces in the Trilateral Euregio Cluster (TEC) with the Institut für Plasmaphysik of the Forschungszentrum Jülich, home of the TEXTOR tokamak, and the Institute for Plasma Physics of the Royal Military Academy in Brussels, as it was realized that further progress required experimentation on a larger tokamak. FOM-Rijnhuizen's major contribution to the TEC collaboration on TEXTOR is a powerful ECRH system consisting of the 110-GHz gyrotron previously installed on RTP and a newly installed 800-kW, >3-s, 140-GHz gyrotron.

After a brief introduction into the principles of ECRH (Sec. II), this paper describes the ECRH installation (Sec. III), and the first results that have been obtained with only the 110-GHz gyrotron (Sec. IV). These results include, in particular, the confirmation of a transport barrier near $q = 1$, the control of sawteeth, and the favorable scaling of ECRH in RI-mode discharges. The conclusions are given in Sec. V together with a perspective on further research.

II. PRINCIPLES OF ECRH

Plasma wave propagation in the electron cyclotron range of frequencies (ECRF) is characterized by two modes of wave propagation as shown in the dispersion diagram[1–3] (Fig. 1). For propagation perpendicular to the magnetic field, these modes are known as the ordinary or O-mode and extraordinary or X-mode. They are characterized by the polarization of the wave electric field, with the polarization of the O-mode being parallel to the magnetic field and the X-mode polarization being perpendicular. The label X-mode or O-mode is generally carried over to the corresponding mode for oblique propagation as well. O-mode dispersion is characterized by a single cutoff at the plasma frequency ω_p. The X-mode has two branches. The fast X-mode branch exists above the upper cutoff, $\omega_+ = (0.25\omega_{ce}^2 + \omega_p^2/(1 - N_\parallel^2))^{0.5} + 0.5\omega_{ce}$, where ω_{ce} is the electron cyclotron frequency and $N_\parallel$ is the parallel refractive index of the waves. The slow branch exists between the lower cutoff, $\omega_- = (0.25\omega_{ce}^2 + \omega_p^2/(1 - N_\parallel^2))^{0.5} - 0.5\omega_{ce}$, and the upper-hybrid resonance, $\omega_{UH} = (\omega_{ce}^2 + \omega_p^2)^{0.5}$. Waves can propagate directly from vacuum into the plasma, where they will be split into the two modes depending on the wave polarization.[3] Waves on the O-mode branch can access the cyclotron resonance $\omega = \omega_{ce}$ as long as the local plasma frequency does not exceed the wave frequency ω. As for the X-mode, only the slow branch provides access to the resonance as long as the lower cutoff does not exceed the wave

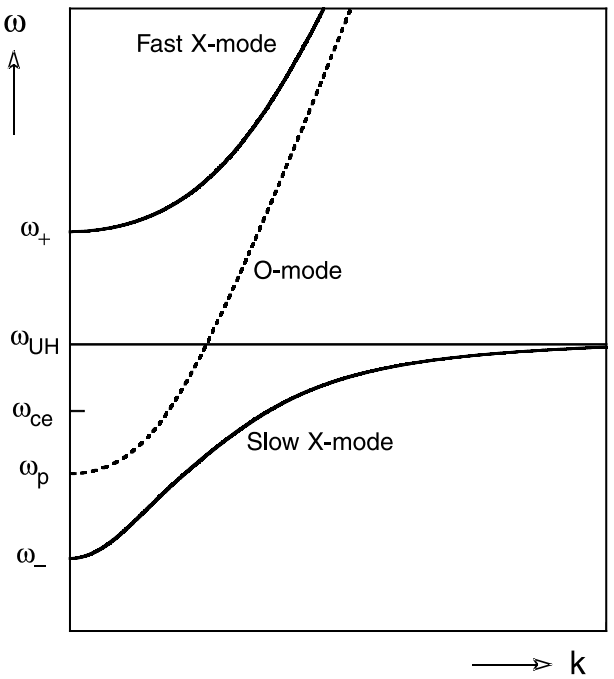

Fig. 1. The dispersion diagram for the propagation of waves in the ECRF.

frequency. Coupling to the slow X-mode is only possible on the high-field side of the cyclotron resonance, i.e., where $\omega_{ce} > \omega$. Access to the second-harmonic resonance is possible on the fast X-mode branch as long as the upper cutoff is low enough.

Wave absorption relies on the wave-particle resonance at the (Doppler-shifted) electron cyclotron frequency or its harmonics:

$$\omega - k_{\parallel} v_{\parallel} = n\omega_{ce} = neB/\gamma m_e \ , \quad n = 1,2,\ldots \ , \qquad (1)$$

where γ is the relativistic mass factor. The resonant wave-particle interaction leads to a predominant increase of the perpendicular energy of resonant electrons.[2] In present-day experiments virtually complete single-pass absorption is achieved for the first- and second-harmonic X-mode and fundamental harmonic O-mode. The power deposition is very localized, often within a few centimeters. In the TEXTOR experiments second-harmonic X-mode waves have been employed almost exclusively.

III. THE TEXTOR ECRH SYSTEMS

The gyrotron is effectively the only available source for high-power, long-pulse millimeter waves as required for ECRH in tokamak plasmas. It is based on the resonant interaction between a selected cavity mode and the gyration of an electron beam as forced by an applied strong magnetic field.[9] This field is generated by a superconducting magnet surrounding the cavity. The high power of modern gyrotrons is achieved through the use of large cavities and high mode numbers of the resonant cavity mode: for example, the $TE_{15,4}$ and $TE_{22,8}$ modes in the case of 110- and 140-GHz gyrotrons at TEXTOR, respectively. An electron beam of ~30 A is accelerated to ~80 kV before it enters the resonant cavity. In the cavity typically ~30 to 40% of the power is extracted from the beam by the resonant cavity mode. The spent beam is then dumped onto the collector, where the remaining energy is dissipated. A first diode-type gyrotron became operational at TEXTOR in 1999 with a frequency of 110 GHz, a pulse length of 200 ms, and a nominal power of 500 kW. It has achieved an electronic efficiency of 35%. The actual power achieved in experiments reported below has been 270 ± 30 kW. The cavity mode is converted internally into a Gaussian beam with >95% efficiency. The non-Gaussian content of the millimeter-wave beam is absorbed near the gyrotron.

In 2002 a second diode-type gyrotron was installed. Its specifications are 140 GHz, 800 kW, and a pulse length of at least 3 s. An electronic efficiency of 38% has been achieved. In first tests on a stone dummy load, the gyrotron exceeded its specifications, and a maximum pulse length of 10 s (equal to the maximum length of a complete TEXTOR discharge) at 670 kW was achieved. The gyrotron is a full continuous wave design, and the pulse length is limited only by the power supply. It is equipped with a chemical vapor deposition (CVD) diamond vacuum window. The extremely low absorption rate for millimeter waves and high thermal conductivity make CVD diamond uniquely suited for high-power millimeter-wave windows. A second CVD diamond window will form the vacuum boundary at the tokamak. An internal converter (97% efficiency) combines with a special matching optics unit (MOU) to create a millimeter-wave beam with >99% Gaussian purity. After the MOU, the beam passes through a meter for transmitted power (MTP) in which 1% of the radiation is diverted by a grating on one of the mirrors for a calorimetric power measurement. A universal polarizer is integrated into the MTP. Detailed descriptions of the ECRH systems are given in Refs. 10, 11, and 12.

III.A. Auxiliary Supplies

The two gyrotrons share a single 80-kV high-voltage power supply capable of 50 A for 10 s, which means that both cannot be operated simultaneously. It consists of a transformer/rectifier unit fed from the 10-kV grid and a modulator/regulator unit. All components have been checked for their long-pulse capability and if necessary are replaced. In particular, a high-pressure water cooling had to be installed on the modulator tetrode.

Whereas the cooling requirements for the 110-GHz gyrotron are modest, those for the 140-GHz gyrotron are very demanding. The medium pressure cooling system for the 110-GHz gyrotron is also used for parts of the 140-GHz gyrotron, as well as all actively cooled components in the transmission line. In addition, the 140-GHz gyrotron is equipped with a high-pressure (8-bar) system for the cavity and power supply tetrode, as well as a low-pressure system for the collector. A dedicated system cools both CVD diamond vacuum windows at the 140-GHz gyrotron and the tokamak.

III.B. Transmission Line and Launcher

Apart from their individual beam forming (MOU) and polarizer units, a confocal quasi-optical transmission line (~25 m) suitable for the transmission of both frequencies transports the waves to the tokamak (see Fig. 2). A switchable mirror allows one to switch between 140- and 110-GHz operation. The transmission line is screened by an aluminum enclosure. At strategic positions inside the enclosure, stray radiation is absorbed by low-flow cooling water in Teflon hoses. The transmission line enters the TEXTOR hall via a dogleg labyrinth. The labyrinth is lined with bricks and also serves as a long-pulse power dump.

Given the size of available CVD diamond windows, the beamline is designed such that a beam waist of 22.8 mm is realized at the torus window. The launcher then consists of a fixed defocusing mirror and a focusing

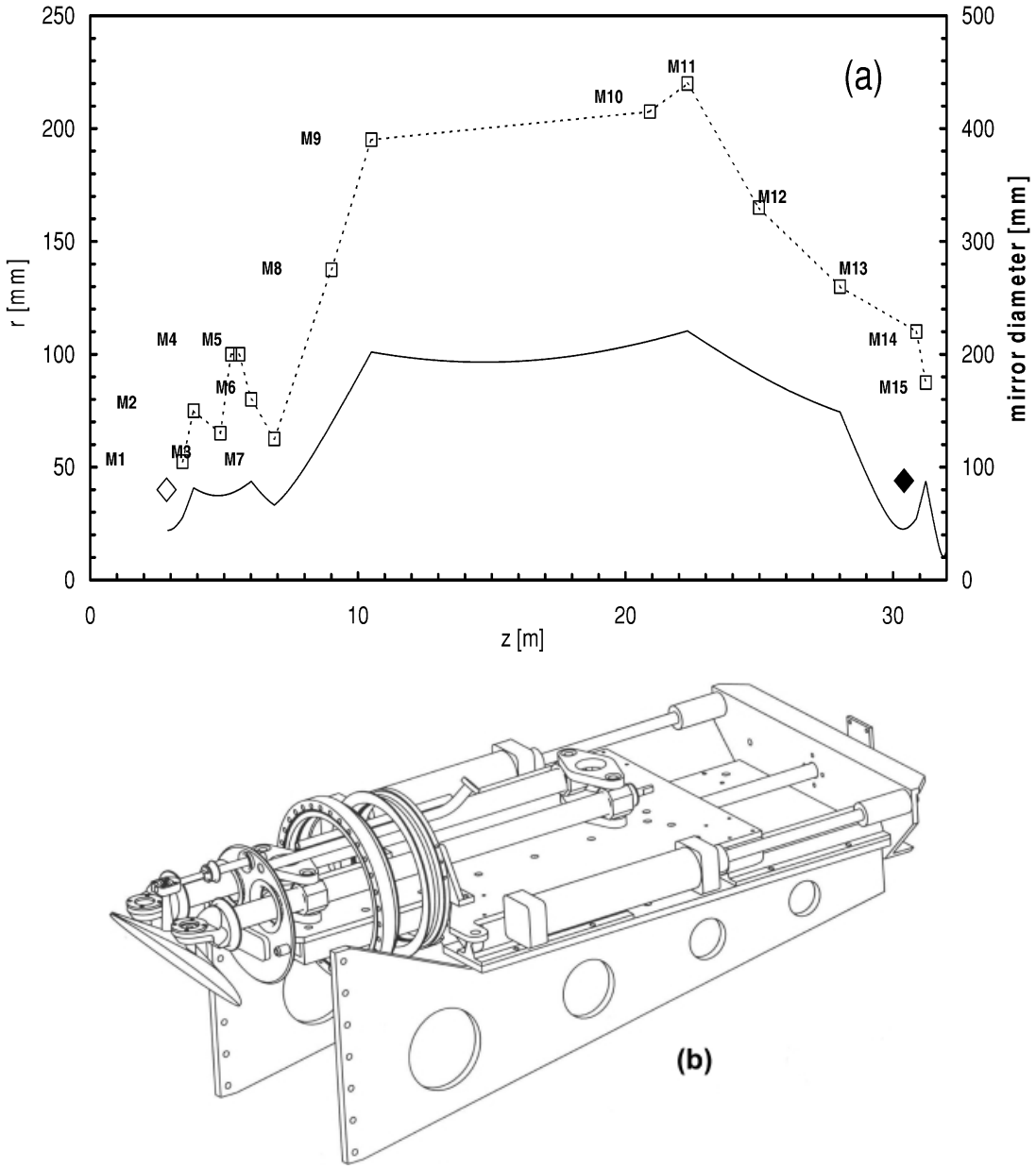

Fig. 2. The quasi-optical transmission system: (a) a schematic overview of the beam waist size (the radius of the spot size at 1/e of the electric field amplitude; full curve, scale to the left), mirror sizes (open squares, scale to the right) along the line. The sizes of the gyrotron and torus vacuum windows are indicated by the diamonds (open and filled, respectively; same scale as mirrors). Mirrors labelled M1 and M2 are part of the 140-GHz MOU, M3 to M6 of the MTP with M4 and M5 forming the universal polarizer. M7 is the switchable mirror for 110- or 140-GHz selection. M8 to M15, launcher mirror, form the shared confocal line. (b) The launcher design. The launcher mirror (on the left) focuses and reflects the microwaves coming from below into the plasma to the left. Moveable rods allow one to tilt the mirror in both the vertical and horizontal planes for poloidal and toroidal steering of the microwave beam, respectively. The launcher is mounted on a rail system, which can be retracted when the system is not in operation to protect the mirror surface from unwanted deposits (for example, during boronization procedures).

final mirror, which can be rotated around both a vertical and horizontal axis. The resulting variation of the toroidal injection angle (−45 to +45 deg) covers injection from cotangential to countertangential with respect to the magnetic field on axis, while the possible variation of the vertical injection angle (−30 to +30 deg) covers the poloidal cross section. The final mirror is positioned at a major radius of 2.365 m in the midplane of the tokamak.

It launches a Gaussian beam into the plasma with a vacuum waist of 1.0 cm (radius of the spot-size at 1/e of the electric field amplitude) being located at $R = 1.74$ m near the axis of the machine. This small focal spot of the beam makes it possible to deposit the wave power very localized into the plasma.

The first experiments reported in Sec. IV, have been performed with a slightly different transmission line and launcher, allowing the same range in injection angles but with slightly different parameters for the Gaussian beam being injected into the plasma: a focus in vacuum with a waist of 1.4 cm at $R = 1.75$ m.

III.C. Control

A comprehensive interlock and protection system has been developed (Fig. 3). In particular the high-power, long-pulse capability of the new 140-GHz gyrotron required the implementation of additional safety measures. For example, firing into an empty torus or a plasma with insufficient absorption is not permissible for long-pulse length, and a protection unit is developed to prevent this (with limited overriding possibilities for preionization experiments). All important protection features are hardwired, but they are interfaced to a programmable logic controller (PLC). The PLC also provides the interface to the installation for remote control from a personal computer in the TEXTOR control room. Both manual (protected) operation and full remote operation are possible.

The data acquisition system is VME based and records diagnostic signals as a function of time (e.g., power, frequency, etc.) as well as the settings of the installation (e.g., launcher angle, polarization, etc.). The data are transferred to a central storage facility and can be accessed using a newly developed protocol, which provides access to all TEXTOR data.[13]

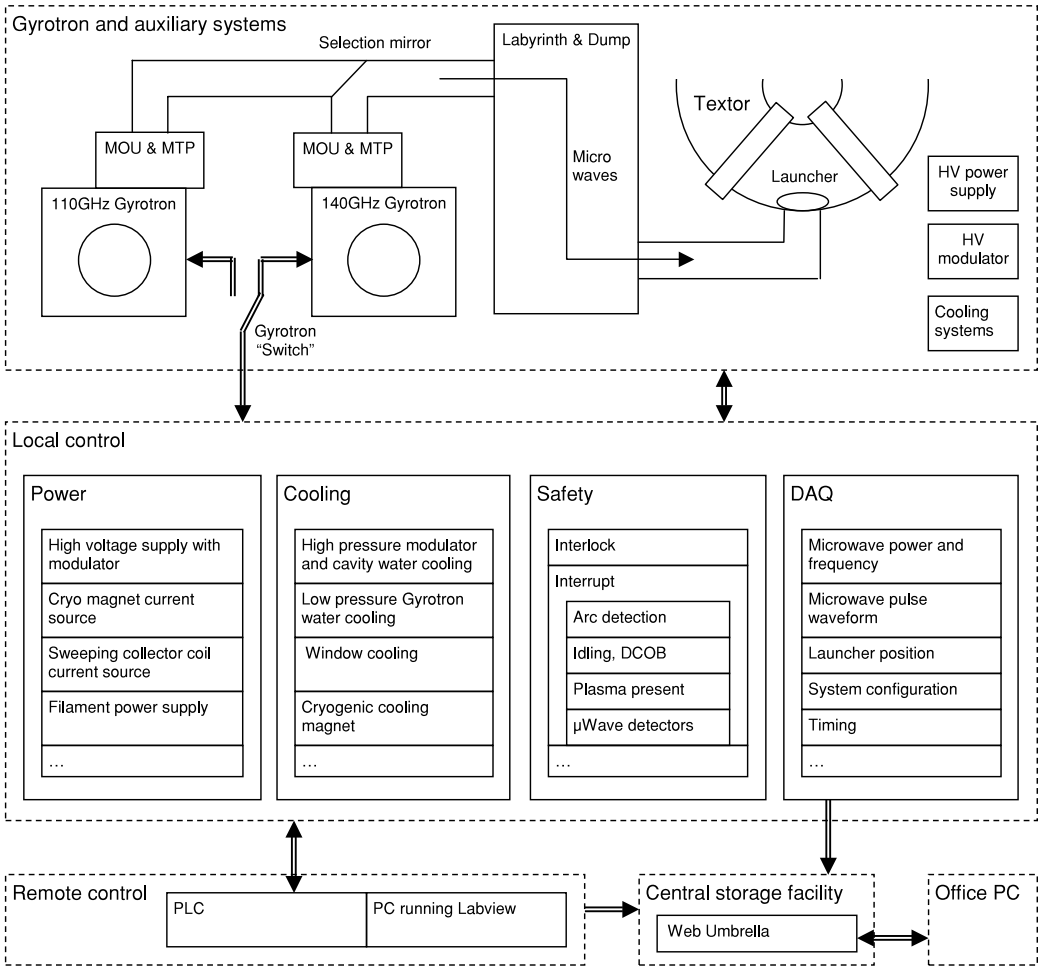

Fig. 3. Schematic overview of the control system. The top section represents the equipment, the central section shows the associated control circuits together with the master unit, and the bottom section shows the computer systems for remote control and data acquisition.

Although the PLC allows convenient control of the installation, it is slow. For fast feedback purposes on the basis of diagnostic signals, it is necessary to have direct access to the timing of gyrotron pulses (e.g., for mode stabilization or dynamic ergotic divertor (DED) diagnostic purposes) and launcher angle (e.g., to track the mode position as it changes in time). Possible direct control is already foreseen in the present control system and will be the subject of further developments.

IV. FIRST RESULTS WITH ECRH ON TEXTOR

In this section we report experimental results on ECRH and collective Thomson scattering (CTS) obtained with the 110-GHz, 200-ms gyrotron (see also Ref. 12). The power injected into the plasma is 270 ± 30 kW.

IV.A. ECRH in RI-Mode

In TEXTOR, plasmas with the best confinement properties are obtained in the so-called radiation improved mode (RI-mode) by the injection of a small amount of radiating species (typically Ne or Ar) in the edge of the plasma.[14,15] Apart from providing a radiating mantle, this impurity injection also leads to peaking of the density profile and suppression of ion temperature gradient turbulence and associated transport.[15] Energy confinement in the RI-mode is characterized by a linear scaling with the line-averaged density $\bar{n}_e$, but it still shows the usual degradation of confinement with total heating power[14]:

$$\tau_{RI} \propto \bar{n}_e P_{tot}^{-2/3} \quad . \tag{2}$$

Although the pulse length of 200 ms is rather limited compared to typical confinement times of ~50 ms in the RI-mode, and the power of only 270 kW is rather small compared to the total heating power of ~2.7 MW in typical RI-mode discharges, first experiments reveal central ECRH in RI-mode plasmas to be remarkably effective[16]: the total stored energy rises in proportion to the full power of central ECRH (see Fig. 4), instead of an efficacy of only 30% as could be expected on the basis of the RI-mode scaling. Moreover, this efficacy of central ECRH is seen to hold for densities right up to the cutoff density for the second-harmonic X-mode at 110 GHz ($n_{cutoff} = 7.5 \times 10^{19}$ m^{-3}, corresponding to a line average density $\langle n_e \rangle \approx 5.5 \times 10^{19}$ m^{-3}).

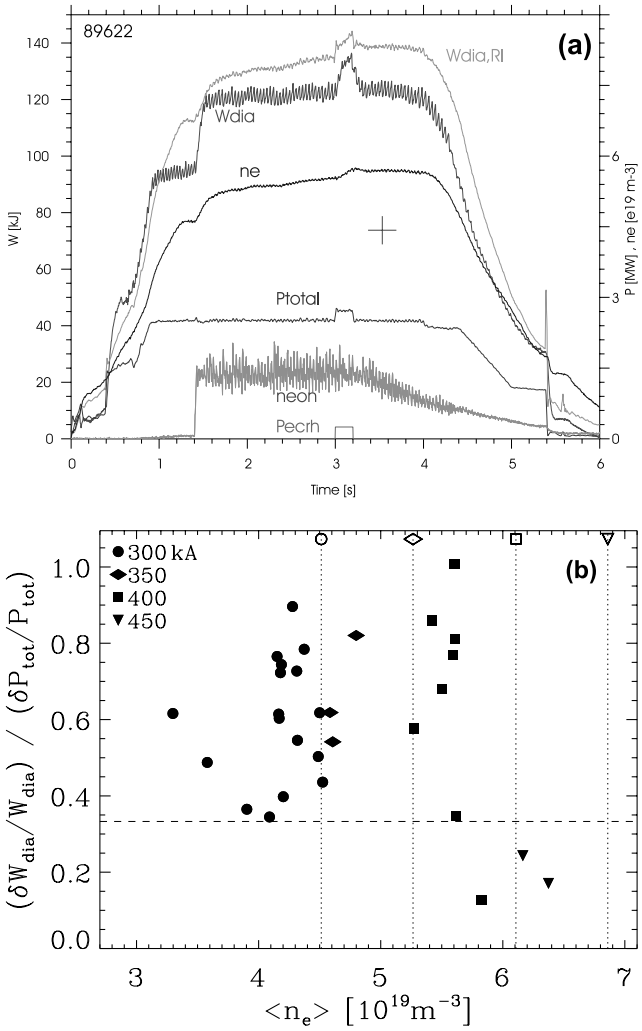

Fig. 4. (a) Evolution of a typical RI-mode discharge with ECRH. The increase of W_{dia} with the injection of Ne signifies the transition to the RI-mode. The curve labeled $W_{dia,RI}$ indicates the expected confined energy W on the basis of the RI-mode scaling.[13] (b) The normalized efficacy, $(\delta W_{dia}/W_{dia})/(\delta P_{tot}/P_{tot})$, of ECRH in RI-mode discharges. The different symbols indicate the plasma current. The dashed line is the efficacy expected by the RI-mode scaling law. The vertical dashed lines indicate the Greenwald density for the four different values of the plasma current. The sharp drop of efficacy near $\langle n_e \rangle \approx 5.5 \times 10^{19}$ m^{-3} is not caused by reaching the Greenwald density limit but is due to reaching the cutoff density.

IV.B. Internal Transport Barriers

Experiments with dominant ECRH in the RTP tokamak have revealed the presence of transport barriers not only at the $q = 1$ surface but also at most low-rational q surfaces.[17] Central ECRH in ohmic TEXTOR discharges clearly shows the presence of an internal transport barrier as well: The central electron temperature shows a sudden drop as the radius of deposition is increased beyond a certain point (by changing the magnetic field; see Fig. 5a). This point is very close to the sawtooth inversion radius, which suggests the association of this transport barrier with $q = 1$. A similar result is obtained for the RI-mode discharges as displayed in Fig. 5b, which shows the efficacy of ECRH in terms of the ratio of the relative

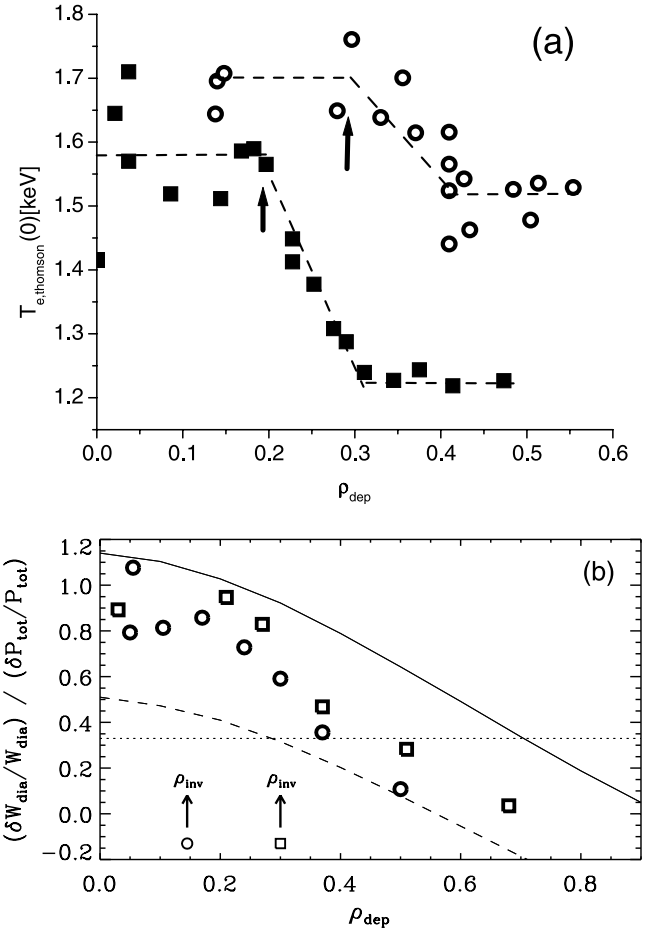

Fig. 5. (a) The central T_e from Thomson scattering as achieved in ohmic target discharges with ECRH as a function of the deposition radius. The ECRH deposition radius is varied by changing the toroidal field. Two data sets are shown for different plasma currents: squares for I_p = 255 kA and circles for I_p = 357 kA. The corresponding densities are $\langle n_e \rangle$ = 2.4 and 1.8 × 10^{19} m^{-3}, respectively. Arrows indicate the respective ohmic sawtooth inversion radii. (b) A similar picture for RI-mode discharges, but now the normalized efficacy, $(\delta W_{dia}/W_{dia})/(\delta P_{tot}/P_{tot})$ is plotted. The data sets shown are for q_a = 3.8, $\langle n_e \rangle$ = 4.0 × 10^{19} m^{-3} (circles) and q_a = 2.9, $\langle n_e \rangle$ = 5.0 × 10^{19} m^{-3} (squares). The full (dashed) line indicates the expected efficacy of ECRH without (with) power degradation, assuming parabolic $\chi_i = \chi_e$ with $\chi_e(0) = 0.6$ and $\chi_e(a) = 3.2$ $m^2 \cdot s^{-1}$. For both data sets a sharp drop of normalized efficacy is observed close to the sawtooth inversion radius (indicated by arrows), i.e., the footprint of a transport barrier in that region. In this series of discharges, the ECRH deposition radius has been varied by changing the poloidal injection angle.

change in total stored energy (measured by the diamagnetic loop) to the relative change in injected power. Although the transition in this case appears less abrupt, the efficacy drops from about unity to below a value of 0.3 as expected in case of the usual degradation of confinement with total heating power. The drop occurs in a broad region near the sawtooth inversion radius. Thus, the high efficacy of ECRH in the RI-mode is associated with a region of reduced transport close to the $q = 1$ surface.

The role of low-order rational q values in the formation of internal barriers has been observed in many other tokamaks (see the review paper[18]). These experiments all required either low (optimized) magnetic shear, or reversed magnetic shear, and in most of the cases, the rational q value played a decisive role only in triggering the barrier. The $q = 1$ barrier presented here, however, occurs for the natural positive magnetic shear in a plasma with only modest velocity shear. No power threshold for the formation (although the minimum applied ECRH power was still 200 kW) nor trigger event could be identified. The clear correlation of the barrier with the sawtooth inversion radius suggests that for these discharges the value of safety factor q rather than its shear is the determining factor for the presence of the barrier.

In further experiments we have probed the internal transport barrier in ohmic target plasmas by means of modulated ECRH (MECH). In a series of similar discharges with MECH, the power deposition radius was scanned by small changes of the toroidal magnetic field. In these discharges (I_p = 350 kA, $q_a \approx 4$, and $\langle n_e \rangle \approx 2 \times 10^{19}$ m^{-3}), eight cycles of MECH were applied, at a frequency of 33.3 Hz and duty cycle $d_c = 0.8$. The second-harmonic electron cyclotron emission (ECE) T_e signals are Fourier analyzed to calculate phases (ϕ) and amplitudes (A) relative to the MECH pulse. Figure 6 shows the first-harmonic phase and amplitude profiles of five TEXTOR discharges of the scan. The rise of amplitudes outside $\rho \approx 0.6$ on the high-field side is most likely due to overlap with the third-harmonic ECE and is neglected in the analysis.

One observes that as ρ_{dep} changes from nearly central to $\rho_{dep} \approx 0.24$, the change in both ϕ and A are only modest. However, going from $\rho_{dep} \approx 0.24$ to 0.36 is seen to cause a sharp transition from a ϕ profile with a low to one with a high central value and a clear off-axis minimum. During this transition, the A profile first remains peaked, while only for larger ρ_{dep} it develops an off-axis maximum. In terms of the electron heat diffusion coefficient (χ_e), this implies a high value inside $\rho \approx 0.24$ and a low value, i.e., a transport barrier, between $\rho \approx 0.24$ and 0.36. The fact that the A profile does not change in parallel with the strong change of the ϕ profile when ρ_{dep} is moved over this narrow region indicates that this barrier might in part be caused by local inward heat convection instead of a low χ_e, as was seen before in RTP (Ref. 8). The high value for the central χ_e might be related to the presence of sawteeth, which for these discharges have a frequency of ~100 Hz, i.e., higher than the modulation frequency. These conclusions are supported by detailed simulations of electron heat transport in these discharges.[12]

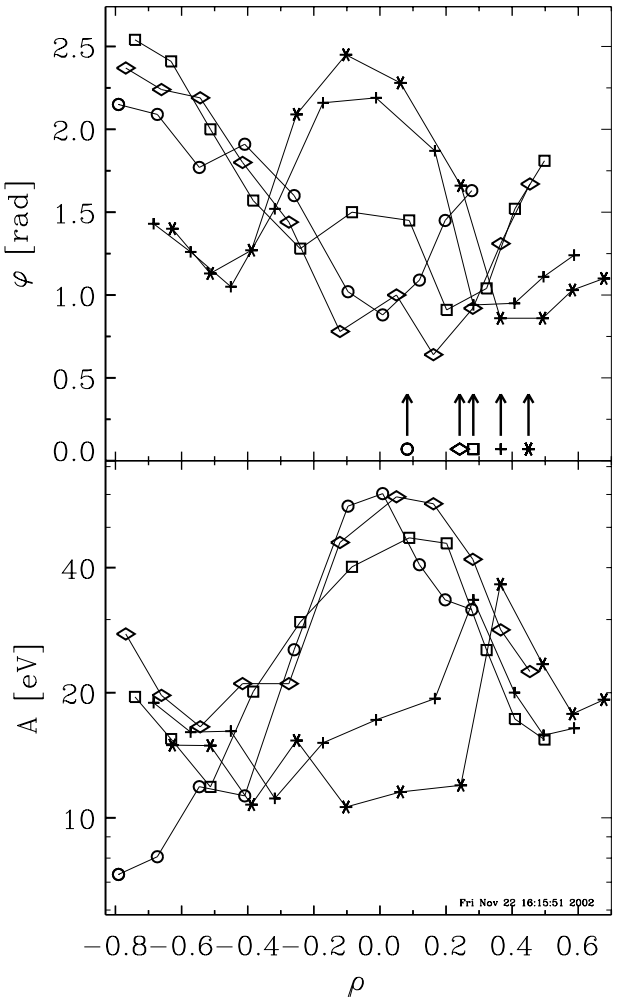

Fig. 6. First-harmonic phase (upper) and amplitude (lower panel) profiles of five similar discharges in which ρ_{dep} (indicated by vertical arrows in the upper panel) was scanned. Plasma parameters: $I_p = 350$ kA, $q_a \approx 4$, and $\langle n_e \rangle \approx 2 \times 10^{19}$ m^{-3}.

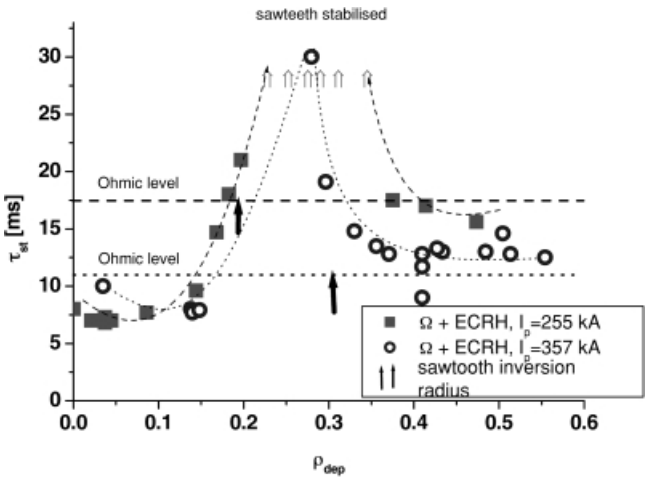

Fig. 7. The central sawtooth period in ohmic discharges with ECRH (270 kW) is shown as a function of the ECRH deposition radius (same data set as Fig. 6a). In the low-current case, complete stabilization ($\tau_{st} \rightarrow \infty$) is obtained with ECRH deposition at or just outside the sawtooth inversion radius in a region ranging from $\rho_{dep} =$ 0.23 to 0.35.

IV.C. Sawtooth Control

Many tokamak experiments with ECRH, starting from the early experiments on T-10 (Ref. 19), have reported on the changes in sawtooth behavior as the ECRH deposition radius is moved through the plasma. A particularly comprehensive study of the effects of ECRH on sawteeth has been reported from TCV (Ref. 20). Also, on TEXTOR the changes in the sawtooth behavior with ECRH have been investigated. Figure 7 shows the sawtooth period in ohmic target plasmas as a function of the ECRH deposition radius. The results are given for two different values of the plasma current with, consequently, two different values of the sawtooth inversion radius. Here, the deposition has been varied by changing the magnetic field from 2.01 T for central deposition to 2.30 T for deposition near midradius. When the heat is deposited inside the sawtooth inversion radius, the sawtooth period decreases, while for deposition at or just outside the sawtooth inversion, the period increases. In case of $I_p =$ 255 kA, even full sawtooth stabilization is obtained for deposition in a relatively broad region outside the inversion radius. In the latter cases, the heating presumably has led to a sufficient broadening of the temperature and current density profiles that a $q = 1$ surface is no longer present in the plasma.

Also, in the RI-mode the sawtooth behavior changes markedly for different deposition radii, as shown in Fig. 8a. In this case the deposition has been varied by changing the poloidal injection angle rather than the toroidal magnetic field. Again, a strong decrease in the sawtooth period is observed with heating inside the inversion radius. However, in the high-current $I_p = 405$ kA case, the picture is complicated as for central deposition the sawteeth change from normal to compound with irregular partial and full collapses as shown in Fig. 8b.

IV.D. Collective Thomson Scattering

The 110-GHz system has also been used as source for a fast ion CTS diagnostic.[21] A number of dedicated experiments have been performed in pursuit of both generic fast ion physics such as fast ion sawtooth sensitivity and confinement time, and specific ion cyclotron resonance heating (ICRH) physics issues intended to challenge and benchmark model calculations. For these experiments TEXTOR is operated at a toroidal field of 2.6 T,

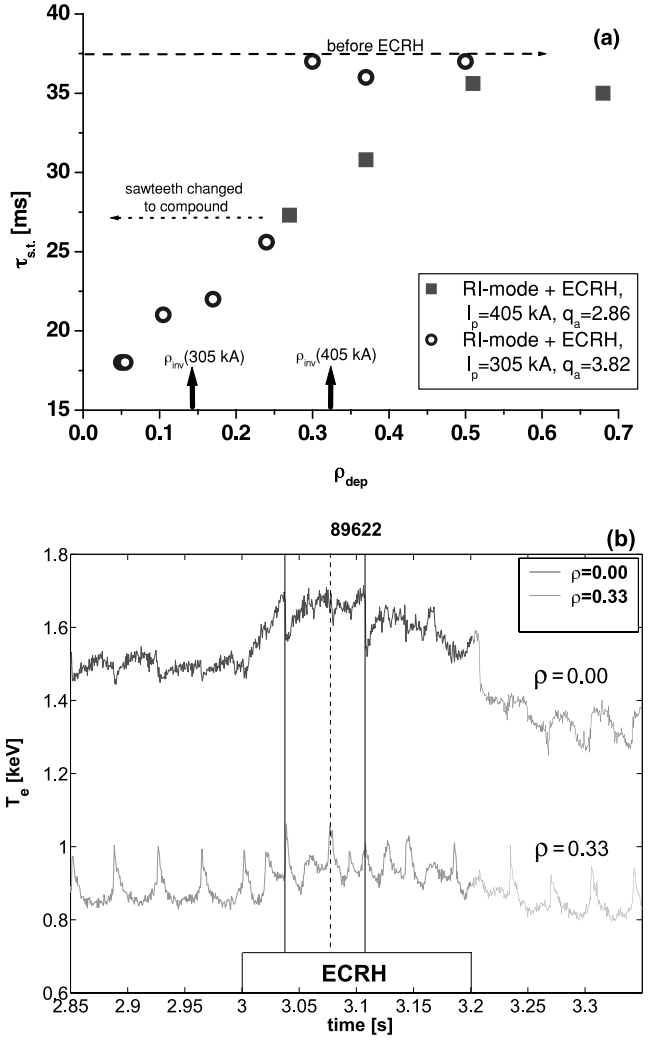

Fig. 8. (a) The sawtooth period in the RI-mode discharges during ECRH as a function of the deposition radius ρ_{dep} (same data set as in Fig. 5b). (b) The transition to compound sawteeth in a high-current (I_p = 405 kA) RI-mode discharge with central ECRH: T_e from ECE is shown corresponding to the center and somewhat outside the sawtooth inversion radius. The full curves indicate two full crashes during ECRH. Various partial crashes are seen outside the inversion radius, which do not (or only slightly as in the case indicated by the dashed line) affect the central temperature.

such that there is no 110-GHz resonance inside the plasma and the 110-GHz probing frequency is between the fundamental and second-harmonic ECE. The diagnostic measures the fast ion population density as a function of a selected velocity component. The signal-to-noise ratio and other constraints permit a velocity space resolution on the order of 10^5 m/s with typically a total of 15 points in the velocity distribution recorded. The spatial resolution is 10 cm radially while the temporal resolution is 4 ms at up to 100 time slices (through modulation of the gyrotron power). The spatial location of the measurement and the direction of the resolved velocity component were varied between shots. Data have been recorded to investigate a broad range of phenomena. In Fig. 9, an example is given that illustrates both redistribution of energetic ions by sawteeth and their slowing down after switch-off of additional heating [neutral beam injection (NBI) plus ICRH]. Both contours of constant phase-space density (a) and time traces for selected velocities (b) are plotted. After the switch-off of the ion heating at 2.2 s, the energetic ion population is seen to decay in ~50 ms, which is in good agreement with the estimated ion slowing-down time due to electron drag (45 ms) (Ref. 22). The effect of sawteeth is clearly seen to be velocity dependent. Measurements from like discharges, in which the orientation of the resolved velocity component and the location of the measurement volume were varied independently, show that the fast ion dynamics at sawtooth collapses is anisotropic as well. More details are reported in Ref. 23.

V. CONCLUSIONS AND PERSPECTIVE

Already the preliminary ECRH experiments on TEXTOR with the 110-GHz gyrotron have provided a wealth of interesting physics results, in spite of the moderate power (270 kW, injected into the plasma) and pulse length (200 ms) of the gyrotron. In particular, central ECRH has proven very effective in RI-mode discharges, which is most likely related to a region of reduced transport near the sawtooth inversion radius or $q = 1$ surface. An electron transport barrier near $q = 1$ is clearly demonstrated in ohmic target plasmas. Modulated ECRH gives further confirmation of the localized nature of this barrier and suggests a possible role of a strong, localized inward energy flux. These results confirm similar observations made previously on the RTP tokamak.[6,8,17] Central ECRH has been shown to result in a strong decrease of the sawtooth period in both ohmic and RI-mode target plasmas. Longer sawtooth periods and even complete stabilization were obtained by ECRH at or just outside the sawtooth inversion radius in ohmic target plasmas. First results have also been obtained from CTS, which already provide many interesting data on fast ion dynamics.

These results, obtained with moderate power and pulse length, hold much promise for the results that will be obtained with the new 140-GHz, high-power, long-pulse-length gyrotron in the fields of electron transport and control of instabilities. With the higher power available, the search for transport barriers and their relation to rational q surfaces can be extended beyond the $q = 1$ surface to other low, rational q surfaces. With the increased current drive capability of the 140-GHz system, transport barriers in optimized reversed shear regimes could also be opened for investigation. An intriguing

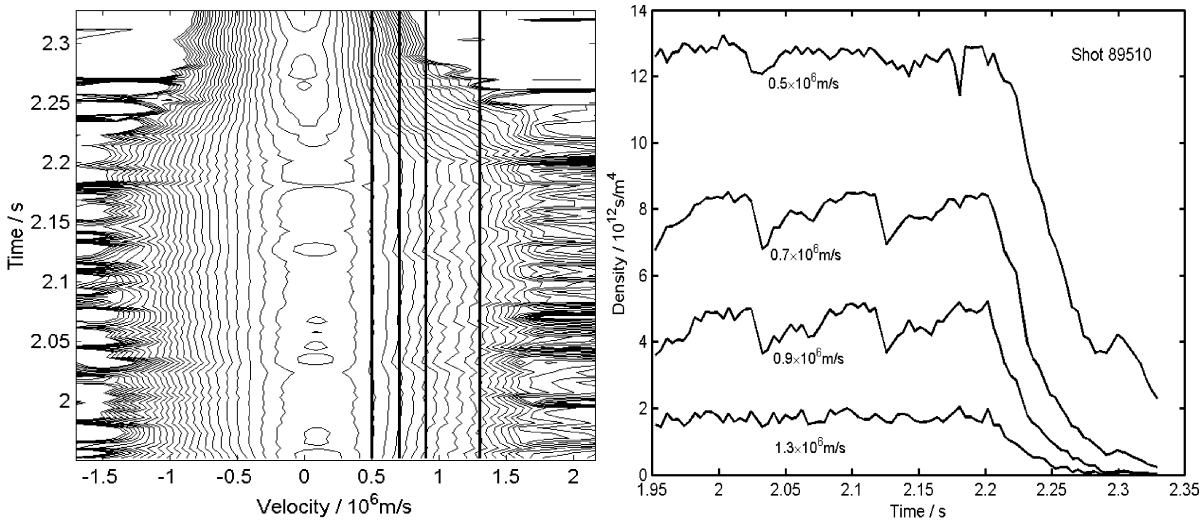

Fig. 9. Both plots show the phase-space density: number of ions per unit volume and unit velocity. In this shot (89510) the resolved velocity component makes an angle of 65.7 deg with the static magnetic field. The measurement volume is just to the high-field side of the plasma center, near the electron density inversion radius. Auxiliary heating (ICRH and NBI) is switched off at 2.2 s. (a) Contours of the logarithm of the ion phase-space density and (b) time traces of the phase-space density for selected velocities.

question to be answered concerning electron transport in the RI-mode is the following: Will the high efficacy of central ECRH hold also for the higher ECRH power? Finally, extensive experiments are being planned in the field of feedback control of instabilities as sawteeth and (neoclassical) tearing modes. Here, also the DED (Ref. 24) plays an important role: It generates in a controlled way the magnetic islands associated with (neoclassical) tearing modes and, thus, allows the study of their interaction with ECRH or ECCD in a well-controlled environment.

ACKNOWLEDGMENTS

This work, supported by the European Communities under the contract of Association between EURATOM/FOM, was carried out within the framework of the European Fusion Programme. The views and opinions expressed herein do not necessarily reflect those of the European Commission.

REFERENCES

1. M. BORNATICI, R. CANO, DE BARBIERI, and F. ENGELMANN, "Electron Cyclotron Absorption and Emission in Fusion Plasmas," *Nucl. Fusion*, **23**, 1153 (1983).

2. V. ERCKMANN and U. GASPARINO, "Review of Electron Cyclotron Resonance Heating and Current Drive in Toroidal Plasmas," *Plasma Phys. Control. Fusion*, **36**, 1869 (1994).

3. R. PRATER, "Heating and Current Drive by Electron Cyclotron Waves," *Phys. Plasmas*, **11**, 2349 (2004).

4. H. HSUAN et al., "Preliminary Results of Electron Cyclotron Heating Experiments on the PDX Tokamak," *Plasma Phys. Control. Fusion*, **26**, 265 (1984).

5. FOM-ECRH TEAM and TFR GROUP, "The Electron Cyclotron Resonance Experiment on TFR," *Nucl. Fusion*, **28**, 1995 (1988).

6. M. R. DE BAAR et al., "Electron Thermal Transport Barrier and Magnetohydrodynamic Activity Observed in Tokamak Plasmas with Negative Central Shear," *Phys. Rev. Lett*., **78**, 4573 (1997).

7. F. SALZEDAS, A. A. M. OOMENS, and F. C. SCHÜLLER, "The Effect of ECRH on the Stability of the Radiation Induced $m = 2$ Mode and on the Current Quench of a Major Disruption," *Nucl. Fusion*, **42**, 881 (2002).

8. P. MANTICA et al., "Heat Convection and Transport Barriers in Low-Magnetic-Shear Rijnhuizen Tokamak Project Plasmas," *Phys. Rev. Lett*., **85**, 4534 (2000).

9. M. THUMM, "State-of-the-Art of High Power Gyro-Devices and Free Electron Masers, Update 2001," FZKA 6708, Forschungzentrum Karlsruhe.

10. J. W. OOSTERBEEK et al., "The ECW Installation at the TEXTOR Tokamak," presented at 22nd Symp. Fusion Technology, Helsinki, Finland, September 9–13, 2002.

11. J. A. HOEKZEMA et al., "The 140 GHz ECW System on TEXTOR," presented at 12th Joint Workshop on ECE and ECRH, Aix-en-Provence, France, May 13–16, 2002.

12. E. WESTERHOF et al., "Electron Cyclotron Resonance Heating on TEXTOR," *Nucl. Fusion*, **43**, 1371 (2003).

13. J. G. KROM et al., "The TEC Web-Umbrella," *Fusion Eng. Des*., **60**, 475 (2002).

14. R. R. WEYNANTS et al., "Overview of Radiative Improved Mode Results on TEXTOR-94," *Nucl. Fusion*, **39**, 1637 (1999).

15. M. TOKAR et al., "Confinement Mechanisms in the Radiatively Improved Mode," *Plasma Phys. Control. Fusion*, **41**, B317 (1999).

16. G. M. D. HOGEWEIJ et al., "Confinement and Transport in EC Heated RI-Mode Discharges in TEXTOR," *Nucl. Fusion*, **44**, 533 (2004).

17. N. J. LOPES CARDOZO, "Electron Thermal Transport in RTP: Filaments, Barriers and Bifurcations," *Plasma Phys. Control. Fusion*, **39** B303 (1997).

18. R. C. WOLF, "Internal Transport Barriers in Tokamak Plasmas," *Plasma Phys. Control. Fusion*, **45**, R1 (2003).

19. R. M. J. SILLEN et al., "Electron Cyclotron Emission Measurements on T-10 with a Grating Polychromator," *Nucl. Fusion*, **26**, 303 (1986).

20. Z. A. PIETRZYK et al., "Behaviour of Central Plasma Relaxation Oscillations During Localized Electron Cyclotron Heating on the TCV Tokamak," *Nucl. Fusion*, **39**, 587 (1999).

21. H. BINDSLEV, "A Quantitative Study of Scattering from Electromagnetic Fluctuations in Plasmas," *J. Atmospheric Terrestrial Phys*., **58**, 98 (1996).

22. H. BINDSLEV et al., "Fast Ion Dynamics in TEXTOR Measured by Collective Thomson Scattering," *Proc. 28th Conf. Controlled Fusion and Plasma Physics*, Funchal, Portugal, June 18–22, 2001, ECA Vol. 25A, 453–456, European Physical Society (2001).

23. H. BINDSLEV et al., "Fast Ion Dynamics Measured by Collective Thomson Scattering of mm Waves," *Proc. 10th Int. Symp. Laser-Aided Plasma Diagnostics*, Fukuoka, Japan, 2001, p. 97 (2001).

24. K. H. FINKEN et al., "Operating Space of the Dynamic Ergodic Divertor for TEXTOR-94," *Nucl. Fusion*, **39**, 637 (1999).